Journal of Alloys and Compounds 651 (2015) 705–711

Contents lists available at ScienceDirect

Journal of Alloys and Compounds

journal homepage: http://www.elsevier.com/locate/jalcom

Local structure study of Fe dopants in Ni–deficit Ni_3Al alloys

V.N. Ivanovski [a, *], A. Umićević [a], J. Belošević–Čavor [a], Hechang Lei [b, 1], Lijun Li [b, 2], B. Cekić [a], V. Koteski [a], C. Petrovic [b]

[a] Laboratory of Nuclear and Plasma Physics, University of Belgrade, Vinca Institute of Nuclear Sciences, P.O. Box 522, 11001, Belgrade, Serbia
[b] Condensed Matter Physics and Materials Science Department, Brookhaven National Laboratory, Upton, NY, 11973, USA

ARTICLE INFO

Article history:
Received 13 March 2015
Received in revised form
24 July 2015
Accepted 20 August 2015
Available online 24 August 2015

Keywords:
Intermetallics
Electronic properties
Hyperfine interactions
Mössbauer spectroscopy
X-ray diffraction

ABSTRACT

The local electronic and magnetic structure, hyperfine interactions, and phase composition of polycrystalline Ni–deficient $Ni_{3-x}Fe_xAl$ ($x = 0.18$ and 0.36) were investigated by means of ^{57}Fe Mössbauer spectroscopy. The samples were characterized by X–ray diffraction and magnetization measurements. The *ab initio* calculations performed with the projector augmented wave method and the calculations of the energies of iron point defects were done to elucidate the electronic structure and site preference of Fe doped Ni_3Al. The value of calculated electric field gradient tensor $V_{zz} = 1.6\ 10^{21}\ Vm^{-2}$ matches well with the results of Mössbauer spectroscopy and indicates that the Fe atoms occupy Ni sites.

1. Introduction

The nickel aluminide Ni_3Al has been attracting considerable attention for several decades. This compound provides performances of primary interest for the turbine, jet engine and furnace industry: it maintains high strength at high temperature, high melting point (~1658 K), high order-disorder transition temperature [1], low density and good resistance to corrosion. The utilization of polycrystalline Ni_3Al for structural applications is limited by its low ductility and by the tendency for intergranular fracture at ambient temperature. The main reason for failure is grain boundary weakness [2–4]. Ni_3Al crystallizes in a $L1_2$ type structure (γ' phase, Cu_3Au-prototype). It is a cubic fcc lattice where Ni(Al) atoms are positioned at face centers (cube corners), making two separate sublattices. Ni_3Al is a weak itinerant ferromagnet. The stoichiometric Ni_3Al has a T_C value of 41.5 K and magnetization of 0.23 μ_B/f.u. (or 0.075 μ_B/Ni) [5]. The ferromagnetic long range order in Ni_3Al disappears ($T_C \rightarrow 0$ K) when the compositional amount of nickel is below 74.5 at. % [5–7].

Solid solutions of Ni_3Al with iron lower material costs and increase strength. Horton et al. have established the solubility limit of Fe in Ni_3Al at less than 15 at. % [8]. The same authors claim that concomitant addition of iron and boron enables better ductility and fabricability of Ni_3Al alloys. It can be argued that a significant ductilization of Ni_3Al is achieved when a third element preferentially substitutes on Ni sublattice [9].

There are indications that for Ni–rich Ni_3Al alloys doped with Fe up to around 2 at. %, Fe atoms exclusively occupy Al sites, irrespective of the matrix composition and annealing temperature [10–13]. For higher Fe content, there are discrepancies if the Fe atoms occupy exclusively Al sites [14,15] or have no site preference [12,16–20].

The thermal history of the sample has strong influence on the Fe site preference for Ni–deficit Ni_3Al alloys [21]. In annealed samples with high Fe content ($\geq$5 at. %), the Fe atoms substitute for both sites [19,21]. The Fe atoms occupy only Ni sites in as–prepared and quenched samples [21].

The Mössbauer spectroscopy is based on the hyperfine interactions of the Fe probe nuclei with the surrounding charges. This makes the ^{57}Fe-Mössbauer effect measurement a particularly sensitive tool for investigation of the local structure and site preference of iron atoms in a material. The Mössbauer studies performed on the Ni–rich $Ni_{3-x}Fe_xAl$ samples showed that the Fe site preference vary with the Fe content [10,12]. In order to clarify Fe site occupancy we have designed our polycrystalline samples as $Ni_{3-x}Fe_xAl$ for

* Corresponding author.
E-mail address: valiva@vin.bg.ac.rs (V.N. Ivanovski).
[1] Present address: Department of Physics, Renmin University of China, Beijing 100872, China.
[2] Permanent address: Key Laboratory of Materials Physics, Institute of Solid State Physics, Chinese Academy of Sciences, Hefei 230031, China.

http://dx.doi.org/10.1016/j.jallcom.2015.08.171
0925-8388/

$x = 0.18$ and $x = 0.36$ ($Ni_{70.5}Fe_{4.5}Al_{25}$ and $Ni_{66}Fe_9Al_{25}$, respectively). Our combined theoretical and experimental studies indicate that Fe preferably occupies Ni sites.

2. Material and methods

Polycrystalline samples of $Ni_{3-x}Fe_xAl$ ($x = 0.18$ and $x = 0.36$) were synthesized by the arc–melting method. Elemental Ni, Fe and Al were used as starting materials. Weight loss during synthesis was less than 0.6% for all samples. The arc–melted ingots were annealed at 800 °C in an evacuated silica ampoule for four days. X–ray diffraction (XRD) patterns on small polycrystalline pieces were taken with Cu K_α radiation ($\lambda = 1.5418$ Å) using a Rigaku Miniflex X–ray machine. The lattice parameters were obtained by refining the unit cell using the RIETICA software [22]. Magnetization measurements were performed in a Quantum Design MPMS–5.

The ^{57}Fe Mössbauer spectra were obtained by constant acceleration in transmission mode using ^{57}Co/Rh source, at 294 K. The spectra calibrated by laser and isomer shifts are presented with respect to the α–Fe foil ($\delta = 0$). Least squares fits were done using the WinNormos/Site software [23]. The Mössbauer line width corrections were calculated by the transmission integral. During the sample preparation for the Mössbauer measurement, a mechanical treatment like ball milling or triturating in an agate mortar was avoided in order to preserve stability of the $L1_2$ ordered structure [24]. The Mössbauer sample holders were filled by pieces which had been obtained from the bulk samples by cutter tools.

Ab initio calculations, based on the augmented plane wave plus local–orbital (APW + lo) method as implemented in the WIEN2k code [25], were carried out in order to verify the experimental results on the hyperfine interactions of the ^{57}Fe nuclei. The WIEN2k calculations were executed for the compositions $Ni_{3-x}Fe_xAl$ for $x = 0.125$ and $x = 0.25$ ($Ni_{71.875}Fe_{3.125}Al_{25}$ and $Ni_{68.75}Fe_{6.25}Al_{25}$), respectively. The conclusions regarding Fe site preference were complemented with DFT calculations of point defect energies, using the VASP program [26,27]. The calculations were done for two cases: (i) when one Ni atom is replaced by Fe – $Ni_{3-x}Fe_xAl$ for $x = 0.125$ ($Ni_{71.875}Fe_{3.125}Al_{25}$) and (ii) when one Al atom is replaced by Fe – $Ni_3Al_{1-y}Fe_y$ for $y = 0.125$ ($Ni_{75}Al_{21.875}Fe_{3.125}$).

3. Results

XRD data of $Ni_{3-x}Fe_xAl$ can be explained by P m −3 m space group of Cu_3Au structure type (Fig. 1) [22,28]. The unit cell refinement yields lattice parameters $a = 0.3573(2)$ nm ($x = 0$), $a = 0.3577(2)$ nm ($x = 0.18$) and $a = 0.3582(2)$ nm ($x = 0.36$), consistent with the expansion of the unit cell as Fe enters the lattice. In addition to the main phase we observed traces of unreacted starting elements Al ($x = 0$) and Ni ($x = 0.18$). The impurity phases are most likely unreacted starting elements Al ($x = 0$) and Ni ($x = 0.18$) whereas rather weak elemental Al peak might also be present in $x = 0.36$ sample similar to $x = 0$.

Low temperature magnetization curves for all samples (Fig. 2(a)) confirm ferromagnetic order. The ordered moment at $T = 1.8$ K is weak (Fig. 2(b)) for $x = 0$ but shows significant enhancement with Fe substitution, in agreement with the paper [5]. The $M(H)$ curves are paramagnetic above T_C's, implying the negligible contribution of extrinsic high temperature magnetic phases. Fig. 3(a–c) shows Arrott plots of $Ni_{3-x}Fe_xAl$ around the inflection points in magnetization curves (Fig. 2(a)) [29]. The estimated Curie temperatures, $T_C = (44 \pm 2)$ K for $x = 0$, $T_C = (194 \pm 2)$ K for $x = 0.18$, and $T_C = (296 \pm 4)$ K for $x = 0.36$ (Fig. 3(d)) are in agreement with the published [30].

The electric field gradient tensor at the ^{57}Fe site is completely described by only two parameters, V_{zz} and $\eta = |(V_{xx}-V_{yy})/V_{zz}|$,

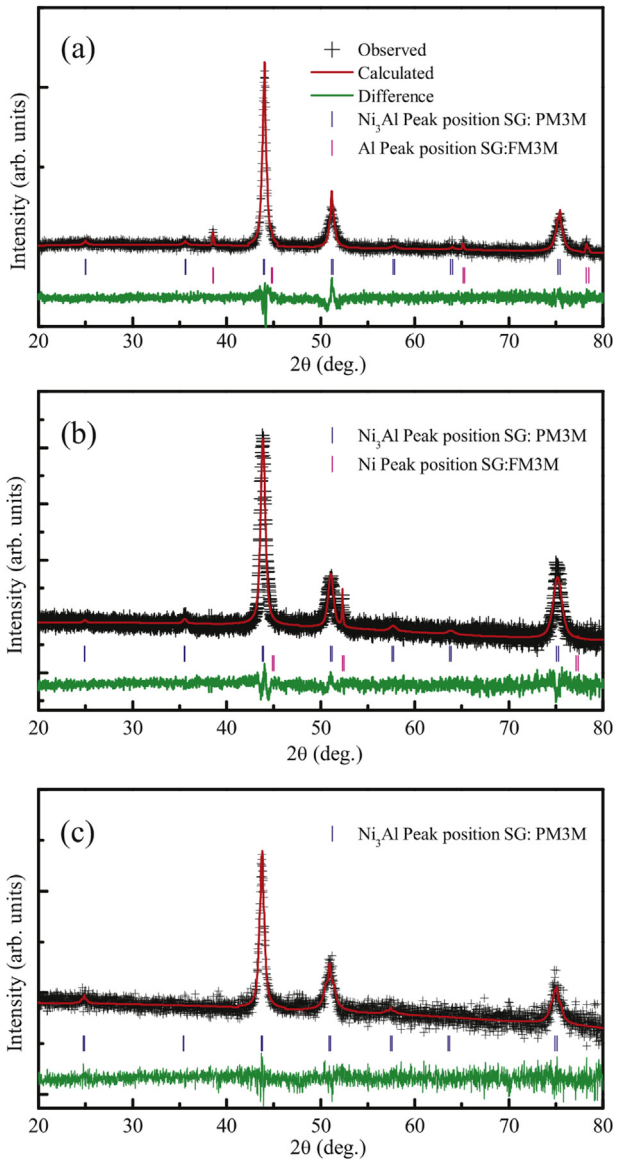

Fig. 1. Powder X–ray diffraction patterns and structural refinement results of $Ni_{3-x}Fe_xAl$: (a) $x = 0$, (b) $x = 0.18$, and (c) $x = 0.36$. The data are shown by (+), the fit is given by the top solid line and the difference curve (bottom solid line) is offset for clarity. Allowed crystallographic reflections are given as vertical tick marks: (a) $L1_2$–Ni_3Al phase (Pm-3m) (top) and fcc–Al impurity phase (Fm-3m) (bottom); (b) $L1_2$–Ni_3Al phase (Pm-3m) (top) and fcc–Ni impurity phase (Fm-3m) (bottom); (c) $L1_2$–Ni_3Al phase (Pm-3m).

when the principal–axes are chosen in such a way that the diagonal components of the *EFG* satisfy the condition $|V_{zz}| \geq |V_{yy}| \geq |V_{xx}|$, i.e. $0 \leq \eta \leq 1$. The two parameters, V_{zz} and η, are coupled in the expression for energy difference $\Delta\epsilon_Q$ between two sublevels of the ^{57}Fe excited $|I = 3/2>$ level [31].

$$\Delta\epsilon_Q = 0.5eQV_{zz}\,(1 + \eta^2/3)^{1/2} \quad (1)$$

The Mössbauer effect measured ^{57}Fe hyperfine parameters are isomer shift δ and quadrupole splitting $\Delta\epsilon_Q$ (in eV). In the ^{57}Fe Mössbauer spectroscopy 1 mms^{-1} is equal to 48.075 neV [31]. The value $Q = 0.16$ b for the ^{57}Fe nuclear quadrupole moment used in Eq. (1), was taken from the calculation of Dufek et al. [32], and supported by the calculation of Wdowik and Ruebenbauer [33].

The dominant doublet is seen in the Mössbauer spectra of

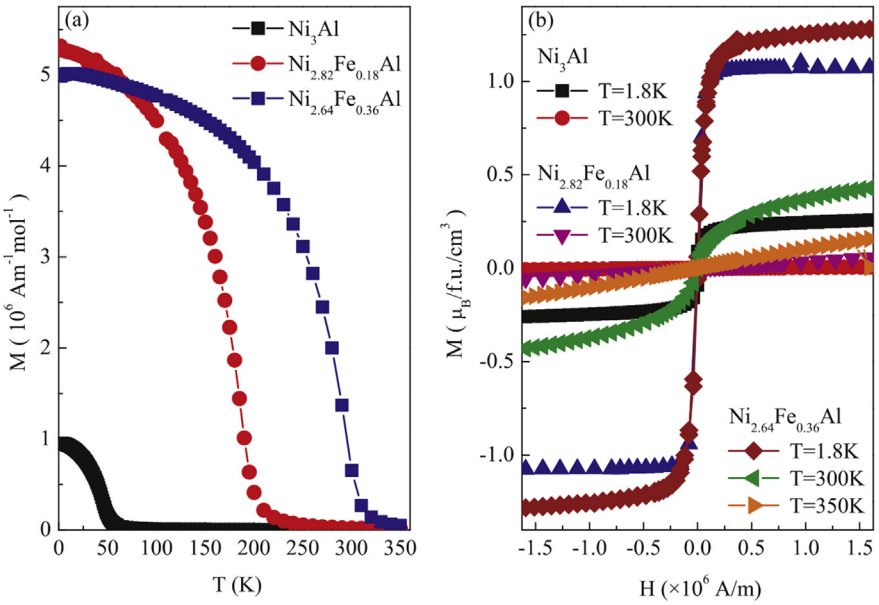

Fig. 2. Temperature dependence of magnetization $M(T)$ measured in 1000 Oe ($\approx 80 \times 10^3 \times$ A/m) (a) and magnetic hysteresis loops (b) for $Ni_{3-x}Fe_xAl$.

$Ni_{3-x}Fe_xAl$ ($x = 0.18$ and 0.36) (Fig. 4). The presence of the dominant doublets indicates the existence of dominant pure electric quadrupole interactions of the ^{57}Fe nuclei in the $Ni_{3-x}Fe_xAl$ alloys. In order to achieve a better fit quality of the spectrum for $x = 0.36$, a single Lorentz line was added. The fitted values of the ^{57}Fe hyperfine parameters of the $Ni_{3-x}Fe_xAl$ ($x = 0.18$ and 0.36) with the corresponding fitted errors are presented in Table 1.

4. Calculation

Ni_3Al crystallizes in the cubic structure (space group Pm-3m). In order to compare the calculated and measured results for $Ni_{3-x}Fe_xAl$, we have constructed $2 \times 2 \times 2$ supercell, starting from the optimized unit cell of Ni_3Al and then we replaced one or two of the Ni host sites by a Fe atom. Thus we obtained the cell closest to the

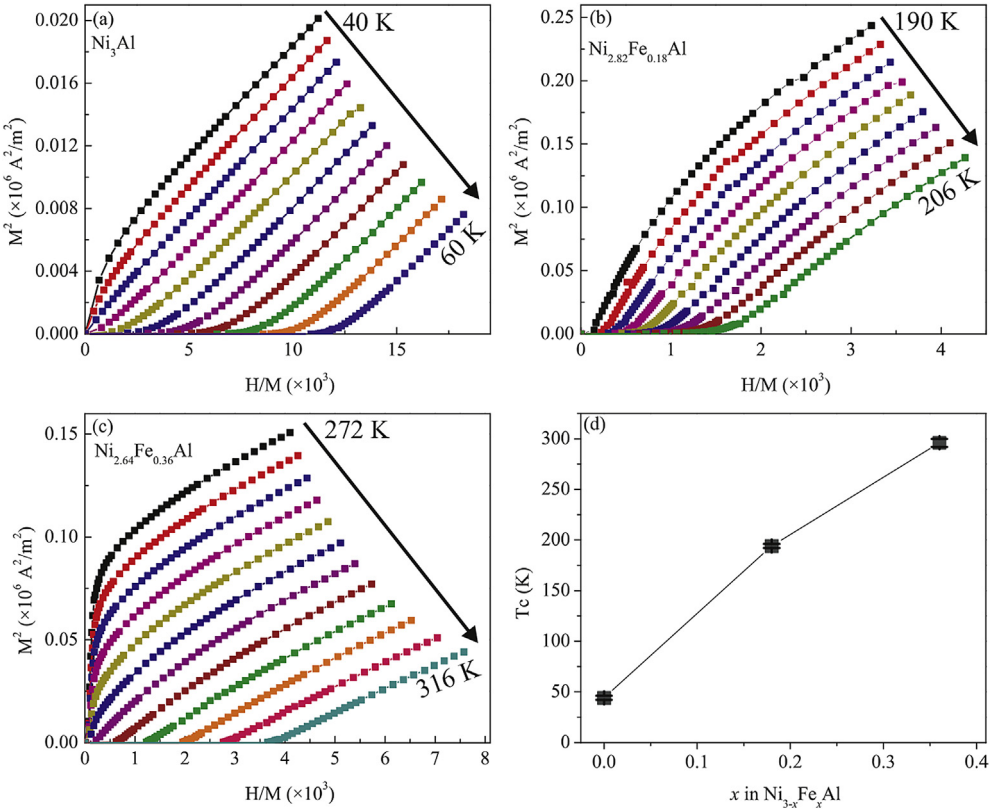

Fig. 3. Arrott plots for $Ni_{3-x}Fe_xAl$ (a–c) and corresponding Curie temperatures T_C (d).

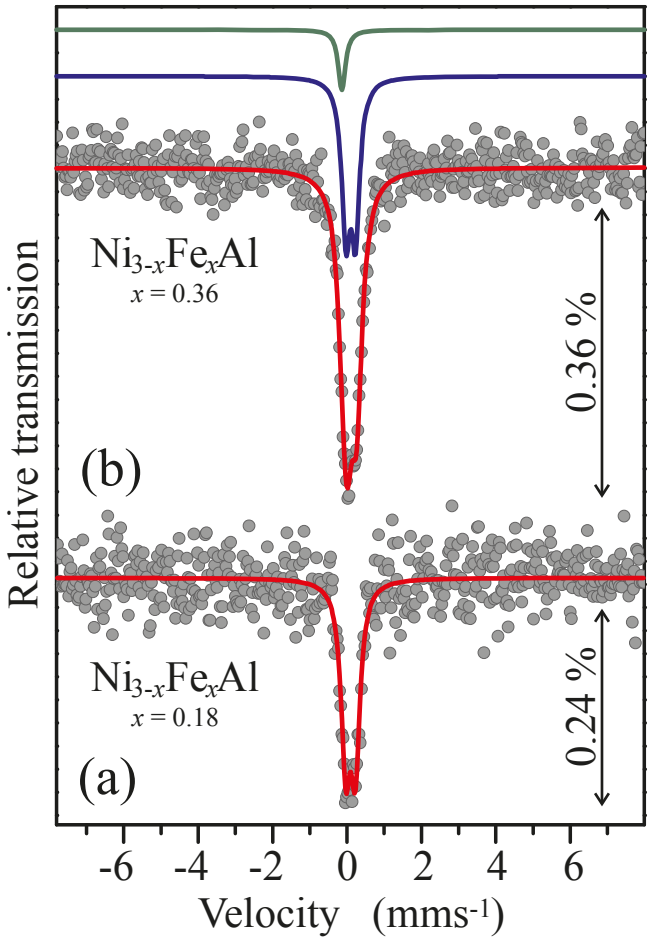

Fig. 4. ^{57}Fe Mössbauer spectra of $Ni_{3-x}Fe_xAl$ at $T = 294$ K: (a) $x = 0.18$ and (b) $x = 0.36$. The data are shown by solid circles and the fit is given by the solid line. Vertical arrow denotes relative position of the lowermost peak with respect to the background. The doublet (red) of the main phase (b), the singlet (dark cyan) and sextet (olive) of the impurity phase (above) are offset for clarity. (For interpretation of the references to colour in this figure legend, the reader is referred to the web version of this article.)

cases of $x = 0.18$ and $x = 0.36$, respectively.

The calculations reported here were performed with the WIEN2k code [25], using a density functional based augmented plane wave plus local orbital (APW + lo) method [34] and the Perdew–Burke–Ernzerhof generalized gradient approximation for the exchange–correlation potential [35]. The threshold energy between valence and core states was −7.1 Ry in order to include the low–laying s states of the 3d elements. The core states were treated fully relativistically, while the valence states were treated within the scalar relativistic approximation. In our supercell calculations the cut–off parameter $R_{mt}K_{max}$ for limiting the number of plane waves was chosen to be 7. The Brillouin zone integration was

Table 1
The fitted Mössbauer hyperfine parameters at 294 K: A – relative area of subspectrum; Γ – line width; δ – the measured isomer shift; $\Delta\epsilon_Q$ – quadrupole splitting (or shift) in unit of mms^{-1}.

$Ni_{3-x}Fe_xAl$	A (%)	Γ (mms^{-1})	δ (mms^{-1})	$\Delta\epsilon_Q$ (mms^{-1})
$x = 0.18$	100	0.20(3)	0.07(1)	0.26(2)
$x = 0.36$	87	0.27(1)	0.10(1)	0.26(1)
	13(5)	0.23(5)	−0.14(2)	

Table 2
The WIEN2k calculated hyperfine parameters: V_{zz} in units of 10^{21} Vm^{-2} and asymmetry parameter η; the magnitude of hyperfine magnetic field B_{hf} in units of T and its decompositions on B^{val} and B^{core}; the calculated magnetic moments μ_{Fe} (per Fe atom) and μ_{cell} (per used cells for the performed calculations) in unit of μ_B for the $Ni_{3-x}Fe_xAl$ for $x = 0.125$ and $x = 0.25$.

$Ni_{3-x}Fe_xAl$	V_{zz} 10^{21} (Vm^{-2})	η	B_{hf} (T)	B^{val} (T)	B^{core} (T)	μ_{Fe} (μ_B)	μ_{cell} (μ_B)
$x = 0.125$	−2.44	0.03	−12.6	54.6	−67.2	2.69	8.43
$x = 0.25$	−2.51	0.02	−13.8	53.4	−67.2	2.69	10.80

achieved via a tetrahedron method [36], using 36 k points in the irreducible wedge of the Brillouin zone. The charge convergence criterion was set to 10^{-5} electron and the maximum force acting on any atom after doping was checked to be less than 10 mRy/a.u. The results are presented in Table 2. The usual convention is to designate the largest component of the EFG tensor as V_{zz}.

The site preference of Fe in the bulk crystal lattice of Ni_3Al was inspected by calculating the energies of iron point defects using the Viena *ab initio* simulation package VASP [26,27]. The calculations were spin polarized, with a cutoff of 300 eV and a force criterion of 0.02 eV/Å. We modeled three different defects, with Fe substituting on Al (Fe_{Al}), Fe substituting on Ni (Fe_{Ni}) and Fe in the interstitial position (Fe_{int}). For the defect calculations we used a supercell of 32 atoms, constructed from the previously relaxed Ni_3Al pure structure in $2 \times 2 \times 2$ geometry. In order to check the convergence of the obtained result we repeated the calculations for the substitutional positions on a larger, $3 \times 3 \times 3$ supercell containing 108 atoms. These calculations showed that the calculated defect energies of Fe_{Ni} and Fe_{Al} converged within 0.015 and 0.003 eV, respectively.

The defect formation energies are calculated from the relation:

$$\epsilon_f = \epsilon_d - \epsilon_{bulk} + \sum n_i\mu_i \quad (2)$$

In this formula, ϵ_{bulk} is the total energy of the supercell without the defect, ϵ_d is the total energy of the relaxed supercell containing the defect atom, n_i is the number of atoms of type i added (negative value) or removed (positive value) from the supercell and μ_i is the chemical potential of the species of type i. In this case, μ_{Fe}, μ_{Ni}, and μ_{Al} are obtained from the calculations of the metal phases of iron, nickel and aluminum.

Fe_{Al} has 12 Ni atoms in the first coordination shell (ICS). The calculated nearest neighbor (NN) bond length of 2.51 Å is shortened by ~0.012 Å with respect to the bulk Ni–Al bond length (2.523 Å). In the Fe_{Ni} lattice position, Fe is surrounded by 8 Ni and 4 Al atoms. We found this position to be much more distorted, with the Fe–Al NN expanded by 0.077 Å and Fe–Ni distances contracted by 0.023 Å. In

Table 3
The Fe valence (4s, 4p, and 3d) decomposed density of states at the Fermi level and the total DOS (the last row) for the $Ni_{3-x}Fe_xAl$ ($x = 0.125$). ($\uparrow + \downarrow$) – the electron population of state in the vicinity of 0 K. ($\uparrow - \downarrow$) – the spin polarization of state. μ – the magnetic moment per the Fe atom.

Fe val. orb.	↑	↓	↑ + ↓	↑ − ↓
4s	0.245	0.231	0.475	0.014
$4p_z$	0.098	0.093	0.191	0.005
$4p_x$	0.087	0.084	0.171	0.004
$4p_y$	0.086	0.082	0.168	0.004
$3d_{xz}$	0.859	0.435	1.294	0.424
$3d_{yz}$	0.862	0.442	1.305	0.420
$3d_{xy}$	0.882	0.316	1.199	0.566
$3d_{z^2}$	0.886	0.354	1.240	0.533
$3d_{x^2-y^2}$	0.898	0.260	1.158	0.637
total/cell	134.851	127.041	261.892	7.811
	$\mu(Fe_{Ni})$: $\sum(\uparrow - \downarrow)^{valence} = 2.607$			

Table 4
The Fe valence (4s, 4p, and 3d) decomposed density of states at the Fermi level and the total DOS (the last row) for the $Ni_3Al_{1-y}Fe_y$ ($y = 0.125$). ($\uparrow + \downarrow$) – the electron population of state in the vicinity of 0 K. ($\uparrow - \downarrow$) – the spin polarization of state. μ – the magnetic moment per the Fe atom.

Fe val. orb.	↑	↓	↑ + ↓	↑ − ↓
4s	0.246	0.230	0.476	0.015
$4p_z$	0.081	0.080	0.161	0.001
$4p_x$	0.079	0.078	0.158	0.001
$4p_y$	0.083	0.083	0.166	0.000
$3d_{xz}$	0.869	0.393	1.261	0.476
$3d_{yz}$	0.889	0.368	1.257	0.522
$3d_{xy}$	0.886	0.369	1.255	0.517
$3d_{3z^2-r2}$	0.926	0.253	1.179	0.673
$3d_{x^2-y^2}$	0.917	0.262	1.179	0.655
total/cell	139.298	129.543	268.841	9.756
	$\mu(Fe_{Al})$: $\sum(\uparrow - \downarrow)^{valence} = 2.861$			

spite of the larger lattice distortion and overall relaxation, our calculations show that Fe is more likely to substitute on the Ni sublattice, with enthalpy of defect formation smaller by 1.15 and 4.5 eV with respect to the Fe_{Al} and Fe_{int} positions, respectively. Interestingly, for the both substitutional positions, we observe a sizable increase of the Fe magnetic moment (Tables 3 and 4) as compared to the value in bulk iron of 2.22 μ_B, whereas for the interstitial position, the magnetic moment of the iron impurity is considerably reduced by the surrounding Ni and Al atoms.

In order to better understand the electronic structure of the Fe doped Ni_3Al, the total and Fe–3d–decomposed density of states (DOS) for both compositions [$Ni_{3-x}Fe_xAl$ and $Ni_3Al_{1-y}Fe_y$ (x, $y = 0.125$)] were calculated by VASP code. Also, the total DOS calculation was carried out in the case of pure γ'–Ni_3Al. The results of the DOS calculations are shown in Figs. 5 and 6. The total and valence decomposed DOS at the Fermi level (ϵ_F) are listed in Tables 3 and 4.

5. Discussion

The symmetry of the Al–site (1a) is a cubic (m-3m) point group. The Fe atoms substituting on the Al sublattice (Fe_{Al}) should not experience any electric quadrupole interaction. However, an electric monopole hyperfine interaction (E_0) related to the chemical isomer shift still remains at Al–site. The Mössbauer experiment cannot resolve it by itself; instead it gives information on the isomer shift which is the sum of the chemical isomer shift and the second order Doppler shift. In the absence of other hyperfine interactions ($\Delta\epsilon_Q = 0$ and $B_{hf} = 0$), the isomer shift is represented in the Mössbauer spectrum as a single line. The (3c)–Ni site has a tetragonal (4/mmm) point group. The ^{57}Fe nucleus at this site should be influenced by an axially symmetric *EFG*. The corresponding pure electric quadrupole interaction of the ^{57}Fe nucleus is matching to a doublet in the Mössbauer spectrum. The existence of any kind of magnetic long–range ordering in the sample, i.e. the presence of the magnetic dipole interaction of the ^{57}Fe nucleus should cause the appearance of at least one sextet in the spectrum.

The dominant doublets visible in the $Ni_{3-x}Fe_xAl$ Mössbauer spectra have the same fitted value of $\Delta\epsilon_Q$–quadrupole splitting, 0.26 mms^{-1} (Table 1), which correspond to the value of the largest principal component of *EFG* tensor, $V_{zz} = 1.6\ 10^{21}\ Vm^{-2}$ (Equation (1) with $\eta = 0$ for (3c)–site). The sign of $\Delta\epsilon_Q$ cannot be determined in Mössbauer spectroscopy. The calculated values of V_{zz}, −2.44 and −2.51 $10^{21}\ Vm^{-2}$ at the Ni site (Table 2), are obtained at 0 K. In general, the $T^{3/2}$ temperature dependence of V_{zz} is often observed in metals [37]. Given this temperature dependence, the decrease of the V_{zz} from 0 K up to room temperature is expected. So, our results

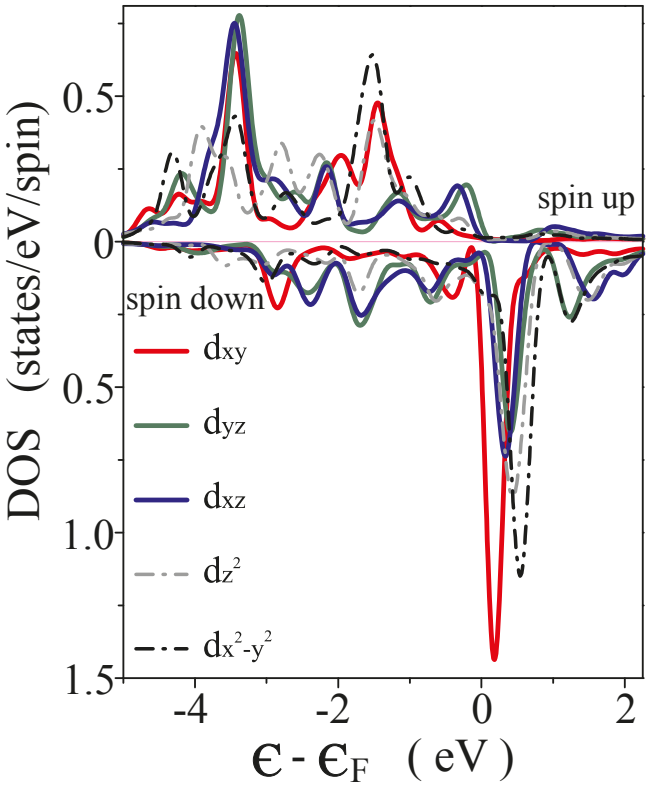

Fig. 5. Spin-resolved partial densities of valence d–states for Fe in $Ni_{3-x}Fe_xAl$ ($x = 0.125$). The (d_{xy}, d_{xz}, d_{yz})–states are shown by the solid lines and ($d_{x^2-y^2}$, d_{z^2})–states are depicted by the dash–dot lines. Energy scales are relative to the energy of Fermi level. Both spins have the same energy scale.

strongly suggest that Fe atoms are positioned on the Ni sublattice in the $Ni_{3-x}Fe_xAl$ alloys. The line width of the dominant doublet in the spectrum for $x = 0.18$ is very small, indicating a well ordered $L1_2$ structure of $Ni_{3-x}Fe_xAl$ ($x = 0.18$) alloy. According to the estimated Curie temperature of $T_C = (296 \pm 4)$ K for the $Ni_{3-x}Fe_xAl$ ($x = 0.36$) alloy, the measurement of the Mössbauer effect in this alloy was

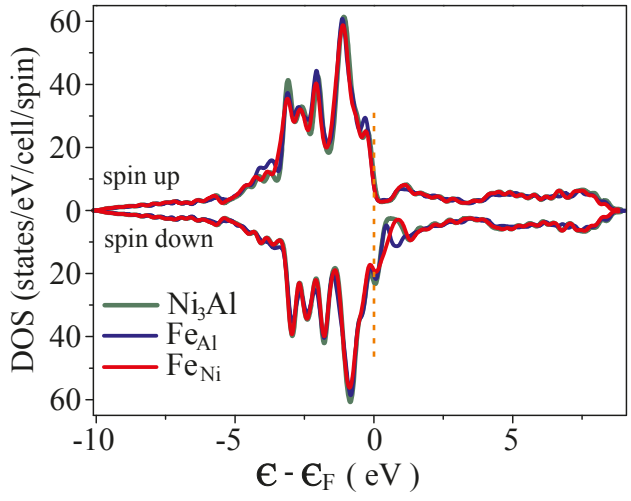

Fig. 6. Spin–resolved total densities of states for Ni_3Al (dark green; lies in the bottom layer); for $Ni_3Al_{1-y}Fe_y$ ($y = 0.125$) (blue; lies in the middle layer); for $Ni_{3-x}Fe_xAl$ ($x = 0.125$) (red; lies in the top layer). (For interpretation of the references to colour in this figure legend, the reader is referred to the web version of this article.)

conducted in the vicinity of the FM transition point. There are still domains of the $L1_2$–$Ni_{3-x}Fe_xAl$ ($x = 0.36$) with nonzero magnetic ordering. The ^{57}Fe nuclei at the 3c–site in the ferromagnetic domains are influenced by an electric quadrupole interaction perturbed with a very weak magnetic dipole interaction. The corresponding Mössbauer spectrum showed the quadrupole doublet with an expanded line width. The total Mössbauer signal is a mix of pure (paramagnetic domains) and perturbed electric quadrupole interactions (ferromagnetic domains). This is the reason for the appearance of broader measured doublet lines in $Ni_{3-x}Fe_xAl$ ($x = 0.36$) [37].

The *ab initio* calculations indicated that the dominant contribution to V_{zz} comes from the polarization of the p–orbitals with some minor contributions from the d–orbitals. Our calculations revealed that, upon substitution of Fe for Ni or Al, there are local distortions around the iron impurity. The first coordination shell of Fe_{Ni} is compressed along the direction perpendicular to the NN Al atoms plane, since the calculated Fe–Ni NN bond lengths were shortened and the Fe–Al NN bonds were elongated. In this configuration, there is an attraction between the NN Ni atoms and the central Fe ion and repulsion between the NN Al atoms and the central Fe ion. On the other hand, for the ICS of Fe_{Al}, the NN Fe–Ni bond lengths were shortened, without any loss of symmetry. It is worth to mention similar result for Fe–Ni bond length obtained in the investigation of $Fe_{46.5}Ni_{53.5}$ and $Fe_{22.5}Ni_{77.5}$ alloys done by Jiang et al. [38]. They found out that the Fe–Ni pairs form strong localized bonds, whereas the Ni–Ni distances are longer. The preference of Fe atoms for a Ni–rich environment has been determined by Deen et al. [10].

The Fe substitute influence can be traced by the Fe–3d–decomposed DOS in the vicinity of the ϵ_F. In the case of Fe_{Ni}, we clearly see from Table 3 a different electron occupation ($\uparrow + \downarrow$) and spin polarization ($\uparrow - \downarrow$) of the Fe valence d–bands. The e_g–bands (d_{xz}, d_{yz}) are more filled and less spin polarized than the d_{xy}–band. The d_{z^2}–band is more populated and less spin polarized than the $d_{x^2-y^2}$–band. There is also a noticeable asymmetry in the electron occupation ($\uparrow + \downarrow$) of the 4p–orbitals (Table 3), which is manifested in the somewhat greater population of the p_z–orbital with respect to the p_x– and p_y–orbitals, as it is expected for the D_{4h} symmetry. This indicates electric polarization of 4p–valence shell. The p–shell polarization is correlated to the compressed first coordination shell. Such ICS electronic configuration of Fe_{Ni} contributes to the rather small $V_{zz}^{valence}$ and $V_{zz}^{lattice}$ at the ^{57}Fe nucleus. We conclude that the Fe dopant elongates its immediate surroundings but does not change the existing D_{4h} symmetry. The principal axis of the D_{4h} symmetry (z'–axis) is parallel to y–axis of the $L1_2$ crystal structure. Nevertheless, as seen from Fig. 5, there is no significant lifting of the degeneracy of the e_g–states (d_{xz}, d_{yz}) (the same applies for the e_u–states (p_x, p_y)).

For Fe_{Al}, the d_{xz}, d_{yz}, and d_{xy} as well as the d_{3z^2-r2} and $d_{x^2-y^2}$ electronic occupations and spin polarizations values are roughly equal (Table 4). It cannot be differentiated between the t_{2g}–bands (and the same is true for the e_g–bands). Therefore, the O_h symmetry at the Fe_{Al} site is intact. In addition, the polarization of 4p–t_{1u}–bands is not present as well. This ICS electronic structure around Fe_{Al} leads to a vanishing EFG. From the valence–decomposed DOS we can conclude that the dominant doublets present in the measured Mössbauer spectra of the $Ni_{3-x}Fe_xAl$ ($x = 0.18$ and 0.36) samples should be ascribed to Fe substitutes located at the Ni site.

The population of 4s–states at 0 K has the same calculated values for Fe_{Ni} in $Ni_{3-x}Fe_xAl$ ($x = 0.125$) and for Fe_{Al} in $Ni_3Al_{1-y}Fe_y$ ($y = 0.125$) (Tables 3 and 4). In general, the difference in the values of the chemical isomer shifts at Fe_{Ni} and Fe_{Al} sites in the $Ni_{3-x}Fe_xAl$ alloy might originate from the screening effect of the p– and d–valence electrons. An increasing electron occupation in the p– and d–valence states decreases the s–electron density at the ^{57}Fe nucleus and increases the value of the chemical isomer shift. The sum of the values of valence 4p– and 3d–electron occupations at 0 K (Tables 3 and 4), in the case of the Fe impurity at the Ni site is $n_{pd}^{v} = 6.726\ e^-$, while for Fe_{Al} it is $6.616\ e^-$. Therefore, the Mössbauer response signal, when Fe substitutes on the Al sites, should be a singlet Lorentz line. The centroid of the singlet line should lay on the position of the isomer shift value of Fe_{Ni} doublet or slightly lower on the velocity axis – such a characteristic singlet was not observed in the measured Mössbauer $Ni_{3-x}Fe_xAl$ spectra at room temperature implying that Fe is not substituting at Al site. Obviously, due to the spin polarization of p– and d–valence states at 0 K, an induction of spin polarization of the s–shells might be expected. Therefore, the creation of the Fermi contact field at the ^{57}Fe nucleus should be obtained at lower temperatures (nuclear Zeeman effect), as measured by Nicholls and Rawlings [12], and Deen et al. [10].

The singlet in the measured Mössbauer spectrum of $Ni_{3-x}Fe_xAl$ for x = 0.36 at room temperature has an isomer shift of −0.14(2) mms^{-1}. In the presence of 30–34 at. % Ni in the fcc Fe–Ni phases, the Mössbauer spectrum consists of a broad sextet and a singlet [39]. We observed very similar singlet in our measurement. Although we did not observe a sextet in the spectrum of $Ni_{3-x}Fe_xAl$ (x = 0.36), we should not exclude the existence of γ–Fe–Ni impurity phases. Due to low data statistics in case of $Ni_{3-x}Fe_xAl$ ($x = 0.36$) we could not reliable detected the mentioned impurities, but this was suggested by our XRD results for $Ni_{3-x}Fe_xAl$ (x = 0.18). Regardless of whether the singlet is attributed either to A2–Fe–Al [40] or γ–Fe–Ni, the obtained value of −0.14(2) mms^{-1} of the isomer shift is sufficiently different from the expected isomer shift of Fe_{Al} (around 0.07 mms^{-1} or slightly larger, Table 1). Hence, the observed singlet cannot be attributed to the $L1_2$ structure. From the foregoing, there is no evidence that the Fe atoms occupy sites on the Al sublattices of the $Ni_{3-x}Fe_xAl$ ($x = 0.18$ and 0.36) samples.

Impurities are observed in the Mössbauer spectrum of the $Ni_{3-x}Fe_xAl$ ($x = 0.36$) sample. The presence of the Fe atoms is also possible in the impurity fcc–$Ni_{1-x}Fe_x$ alloy found by XRD in $Ni_{3-x}Fe_xAl$ ($x = 0.18$) sample; however it is not detected by the Mössbauer spectroscopy. One possible reason is that its relative small amount could not be detected due to bad count statistics.

Fig. 6 presents the total DOS calculated for Ni_3Al, $Ni_3Al_{1-y}Fe_y$ for $y = 0.125$, and $Ni_{3-x}Fe_xAl$ for $x = 0.125$. The small difference in the calculated DOS is visible from the Fermi level up to 1.15 eV above the Fermi level. A spin polarized conduction band occurs within this energy range enabling the ferromagnetic ordering of the sample. The values of total DOS at the ϵ_F are 10.713, 7.826, and 7.754 for spin up, and 22.716, 20.485, and 18.925 for spin down, respectively. The calculated DOS at the Fermi level for the mentioned alloys confirms that they are weak ferromagnets in the vicinity of 0 K. According to the calculated total DOS at the ϵ_F, the $Ni_{3-x}Fe_xAl$ for $x = 0.125$ alloy is more stable than the Ni_3Al, $Ni_3Al_{1-y}Fe_y$ ($y = 0.125$) alloys. This also supports our conclusion that the Fe impurity prefers Ni sites in the $L1_2$–Ni_3Al.

Considering the magnetic moment per Fe atom, our calculations give a value of 2.861 μ_B for Fe_{Al}, and a value of 2.607 μ_B for Fe_{Ni}. The larger spin polarization of 3d–states calculated for Fe_{Al} produces larger magnetic moment then the one for Fe_{Ni}.

6. Conclusions

We have used the Mössbauer spectroscopy to address Fe site preference in the annealed $Ni_{3-x}Fe_xAl$ ($x = 0.18$ and 0.36) alloys at ambient temperature. Our investigation indicates that the Fe atoms substitute at Ni sites, in agreement with calculated energies of

defect formation. This results in local anisotropy distortions around the iron impurity. No significant lifting of the Fe 3d–e_g and 4p–e_u – states degeneracy implies conservation of the local D_{4h} symmetry. The first coordination shell of substituted Fe on Ni site is increased and compressed perpendicular to nearest neighbor plane of Al atoms.

While the sample with lower Fe content is completely paramagnetic at 296 K, the other sample ($x = 0.36$) exhibits domains with nonzero magnetic ordering, which can be observed, but not measured in Mössbauer spectrum. The hyperfine parameters of the measured doublets are in good agreement with calculation.

Acknowledgments

This work has been supported by the grant No. 171001 from the Ministry of Education, Science and Technological Development of the Republic of Serbia. Work at Brookhaven is supported by the US DOE under contract No. DE–AC02–98CH10886.

References

[1] R.W. Cahn, P.A. Siemers, J.E. Geiger, P. Bardhan, Acta. Metall. 35 (11) (1987) 2737–2751, http://dx.doi.org/10.1016/0001-6160(87)90273-2.
[2] C.T. Liu, J.O. Stiegler, Science 226 (1984) 636–642, http://dx.doi.org/10.1126/science.226.4675.63.
[3] K. Aoki, O. Izumi, T. Jpn. I. Met. 19 (4) (1978) 203–210. www.jim.or.jp/journal/e/pdf3/19/04/203.pdf.
[4] C.T. Liu, Scr. Metall. Mater. 27 (1) (1992) 25–28, http://dx.doi.org/10.1016/0956-716X(92)90313-4.
[5] F.R. De Boer, C.J. Schinkel, J. Biesterbos, S. Proost, J. Appl. Phys. 40 (3) (1969) 1049–1055.
[6] S.N. Kaul, A. Semwal, J. Phys. Condens. Matter 16 (47) (2004) 8695–8712, http://dx.doi.org/10.1088/0953-8984/16/47/020.
[7] P.D. Hambourger, R.J. Olwert, C.W. Chu, Phys. Rev. B 11 (9) (1975) 3501–3503, http://dx.doi.org/10.1103/PhysRevB.11.3501.
[8] J.A. Horton, C.T. Liu, M.L. Santella, Metall. Trans. A 18 (7) (1987) 1265–1277, http://dx.doi.org/10.1007/BF02647196.
[9] A. Chiba, S. Hanada, S. Watanabe, Scr. Metall. Mater 25 (2) (1991) 303–307, http://dx.doi.org/10.1016/0956-716X(91)90183-2.
[10] J.K. van Deen, J.W. Drijver, F. van der Woude, Phys. B + C 86–88 (1) (1977) 397–398, http://dx.doi.org/10.1016/0378-4363(77)90362-X.
[11] A. Almazouzi, H. Numakura, M. Koiwa, K. Hono, T. Sakurai, Intermetallics 5 (1) (1997) 37–43, http://dx.doi.org/10.1016/S0966-9795(96)00064-7.
[12] J.R. Nicholls, R.D. Rawlings, Acta Metall. 25 (2) (1977) 187–194, http://dx.doi.org/10.1016/0001-6160(77)90122-5.
[13] M. Balasubramanian, R. Lyver, J.I. Budnick, D.M. Pease, Appl. Phys. Lett. 71 (3) (1997) 330–332 (Accession Number: 4250786).
[14] K. Lawniczak–Jablonska, R. Wojnecki, J. Kachniarz, J. Phys. Condens. Matter 12 (10) (2000) 2333–2350, http://dx.doi.org/10.1088/0953-8984/12/10/317.
[15] S. Pascarelli, F. Boscherini, S. Mobilio, K. Lawniczak–Jablonska, R. Kozubski, Phys. Rev. B 49 (21) (1994) 14984–14990, http://dx.doi.org/10.1103/PhysRevB.49.14984.
[16] H.F. Sluiter Marcel, M. Takahashi, Y. Kawazoe, Acta Mater 44 (1) (1996) 209–215, http://dx.doi.org/10.1016/1359-6454(95)00143-1.
[17] A.V. Ruban, H.L. Skriver, Phys. Rev. B 55 (2) (1997) 856–874, http://dx.doi.org/10.1103/PhysRevB.55.856.
[18] S. Ochiai, Y. Oya, T. Suzuki, Acta Metall. 32 (2) (1984) 289–298, http://dx.doi.org/10.1016/0001-6160(84)90057-9.
[19] D. Shindo, M. Kikuchi, M. Hirabayashi, S. Hanada, O. Izumi, T. Jpn. I. Met. 29 (12) (1988) 956–961. www.jim.or.jp/journal/e/29/12/956.html.
[20] Y.P. Wu, N.C. Tso, J.M. Sanchez, J.K. Tien, Acta Metall. 37 (10) (1989) 2835–2840, http://dx.doi.org/10.1016/0001-6160(89)90318-0.
[21] B. Annie D'Santhoshini, S.N. Kaul, J. Phys. Condens. Matter 15 (29) (2003) 4903–4918, http://dx.doi.org/10.1088/0953-8984/15/29/302.
[22] B. Hunter, Rietica-a visual Rietveld program, Int. Union. Crystallogr. Newsl. 20 (1998) 21. http://www.iucr.org/iucr-top/comm/cpd/Newsletters/.
[23] R.A. Brand, WinNormos Mössbauer Fitting Program, Universität Duisburg, Duisburg, Germany, 2008 [software].
[24] H. Bakker, G.F. Zhou, H. Yang, Prog. Mater. Sci. 39 (3) (1995) 159–241, http://dx.doi.org/10.1016/0079-6425(95)00001-1.
[25] P. Blaha, K. Schwarz, G.K.H. Madsen, D. Kvasnicka, J. Luitz, WIEN2k an Augmented Plane Wave Plus Local Orbitals Program for Calculating Crystal Properties, Vienna University of Technology, Vienna, Austria, 2001 [software].
[26] G. Kresse, J. Furthmüller, Comp. Mater. Sci. 6 (1) (1996) 15–50, http://dx.doi.org/10.1016/0927-0256(96)00008-0.
[27] G. Kresse, J. Furthmüller, Phys. Rev. B 54 (1996) 11169–11186, http://dx.doi.org/10.1103/PhysRevB.54.11169.
[28] S. Députier, R. Guérin, Y. Ballini, A. Guivarc'h, J. Alloy. Compd. 217 (1) (1995) 13–21, http://dx.doi.org/10.1016/0925-8388(94)01296-T.
[29] A. Arrott, Phys. Rev. 108 (6) (1957) 1394–1396, http://dx.doi.org/10.1103/PhysRev.108.1394.
[30] J.R. Thompson, H.R. Kerchner, S.T. Sekula, J. Magn. Magn. Mater 54–57 (2) (1986) 1069–1070, http://dx.doi.org/10.1016/0304-8853(86)90385-9.
[31] Y.-L. Chen, D.-P. Yang, Mössbauer Effect in Lattice Dynamics, Wiley-VCH Verlag GmbH & Co. KGaA, Weinheim, 2007, ISBN 978-3-527-40712-5.
[32] P. Dufek, P. Blaha, K. Schwarz, Phys. Rev. Lett. 75 (19) (1995) 3545–3548, http://dx.doi.org/10.1103/PhysRevLett.75.3545.
[33] U.D. Wdowik, K. Ruebenbauer, Phys. Rev. B 76 (2007), http://dx.doi.org/10.1103/PhysRevB.76.155118, 155118–1–6.
[34] A.R. Williams, J. Kubler Jr., C.D. Gelatt, Phys. Rev. B 19 (12) (1979) 6094–6118, http://dx.doi.org/10.1103/PhysRevB.19.6094.
[35] J.P. Perdew, K. Burke, M. Ernzerhof, Phys. Rev. Lett. 77 (18) (1996) 3865–3868, http://dx.doi.org/10.1103/PhysRevLett.77.3865.
[36] P.E. Blochl, O. Jepsen, O.K. Andersen, Phys. Rev. B 49 (23) (1994) 16223–16233, http://dx.doi.org/10.1103/PhysRevB.49.16223.
[37] K. Szymanski, W. Olszewski, D. Satula, L. Dobrzynski, K. Brzozka, J. Jankowska–Kisielinska, J. Phys. Soc. Jpn. 78 (12) (2009), http://dx.doi.org/10.1143/JPSJ.78.124708, 124708–1–7.
[38] X. Jiang, G.E. Ice, C.J. Sparks, L. Robertson, P. Zschack, Phys. Rev. B 54 (5) (1996) 3211–3226, http://dx.doi.org/10.1103/PhysRevB.54.3211.
[39] Y. Nakamura, M. Shiga, N. Shikazono, J. Phys. Soc. Jpn. 19 (7) (1964) 1177–1181, http://dx.doi.org/10.1143/JPSJ.19.1177.
[40] W. Deng, X.-X. Sun, S.-X. Tan, Y.-X. Li, D.-K. Xiong, Y.-Y. Huang, Chin. Phys. C 37 (2013) 128201–1–5, http://dx.doi.org/10.1088/1674-1137/37/12/128201.